Inorganic Chemistry

FORUM ARTICLE

pubs.acs.org/IC

Designing Catalysts for Nitrene Transfer Using Early Transition Metals and Redox-Active Ligands

Alan F. Heyduk,* Ryan A. Zarkesh, and Andy I. Nguyen

Department of Chemistry, University of California, Irvine, California 92697-2025, United States

Supporting Information

ABSTRACT:

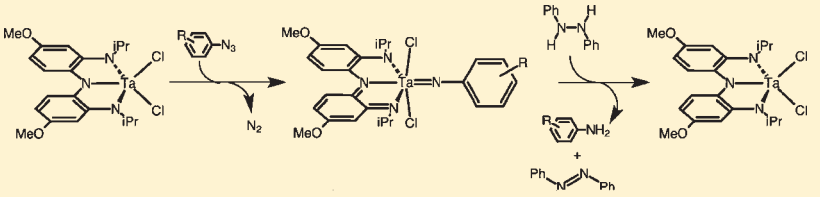

In this Forum Article, we discuss the use of redox-active pincer-type ligands to enable multielectron reactivity, specifically nitrene group transfer, at the electron-poor metals tantalum and zirconium. Two analogous ligand platforms, [ONO] and [NNN], are discussed with a detailed examination of their similarities and differences and the structural and electronic constraints they impose upon coordination to early transition metals. The two-electron redox capabilities of these ligands enable the transfer of organic nitrenes to tantalum(V) and zirconium(IV) metal centers despite formal d^0 electron counts. Under the correct conditions, the resulting metal imido complexes can participate in further multielectron reactions such as imide reduction, nitrene coupling, or formal nitrene transfer to an isocyanide.

I. INTRODUCTION

Early-Transtion-Metal Imido Complexes. Early-transition-metal imido complexes have attracted interest for the impressive stoichiometric bond-activation reactions they can perform.[1−4] Cyclopentadienylzirconium imido complexes provide an example of these bond-activation reactions including [2 + 2] cycloadditions with alkynes, alkenes, imines, and isocyanides, as summarized in Chart 1.[5] C−H bond activation of aromatic and aliphatic hydrocarbons is also possible with group IV imido complexes. While $Cp_2Zr{=}NR$ complexes readily activate the C−H bond of benzene to afford $Cp_2Zr(Ph)(NHR)$ derivatives,[6] transient three-coordinate $(silox)_2M(=NR)$ complexes (M = Ti, Zr; $silox^-$ = tri-*tert*-butyl siloxide) can activate both aromatic and aliphatic C−H bonds, including those of methane, under mild conditions.[7,8] A key aspect of the exceptional reactivity displayed by $(silox)_2M(=NR)$ is polarization of the metal−imido bond. Juxtaposition of an electropositive zirconium or titanium metal with an electronegative nitrene nitrogen leads to a highly polarized M=NR bond, which, in turn, strongly polarizes the substrate C−H bond for activation.[9] In short, the electron-rich imido moiety accepts a proton from the hydrocarbon, while the electron-poor metal accepts the alkyl group. In the case of group V imido complexes, less bond polarization leads to less reactive complexes;[10] however, these imido species still display impressive bond-activation chemistry and continue to be of interest as potential intermediates in homogeneous N_2 reduction schemes.[11−16]

While the bond-activation chemistry of early-transition-metal imido complexes has been exploited in the development of some catalytic reactions, typically the overall transformations are nitrene-exchange reactions (redox-neutral) rather than nitrene-transfer reactions (formal oxidations) owing to the inability of the early transition metals to accommodate multielectron changes in the oxidation state. For example, the reaction of an alkene with a zirconium imido complex by a [2 + 2] cycloaddition pathway forms a metalloazocyclobutane species, which can eliminate an amine by protonolysis, regenerating the zirconium imide and allowing for catalytic olefin hydroamination.[17] While olefin hydroamination by this pathway is not common, there have been extensive reports of catalytic alkyne hydroaminations that follow this route. In both olefin and alkyne hydroamination, the overall transformation is a nonredox process as the product amine is in the same oxidation state as the substrate and the metal center stays in the zirconium(IV) oxidation state throughout the process. In contrast, a two-electron redox reaction from the same metalloazocyclobutane species would generate an aziridine by nitrene transfer to the olefin (a formal oxidation of the double bond). Such reactivity has not been observed for zirconium imido complexes owing to the reluctance of zirconium(IV) to undergo reductive elimination reactivity. In a few specific cases, two-electron nitrene- or nitride-transfer chemistry has been observed for group V metals, where access to both the 3+ and 5+ oxidation states is possible.[18,19] To our knowledge, parallel chemistry with group IV metals has not been reported, yet given the bond-activation reactions summarized in Chart 1, accessible redox reactivity that allows two-electron group transfer from

Received: May 1, 2011
Published: July 20, 2011

Chart 1

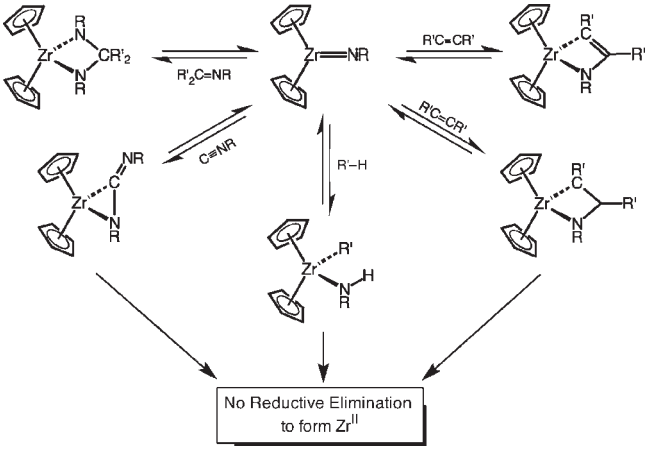

Chart 2

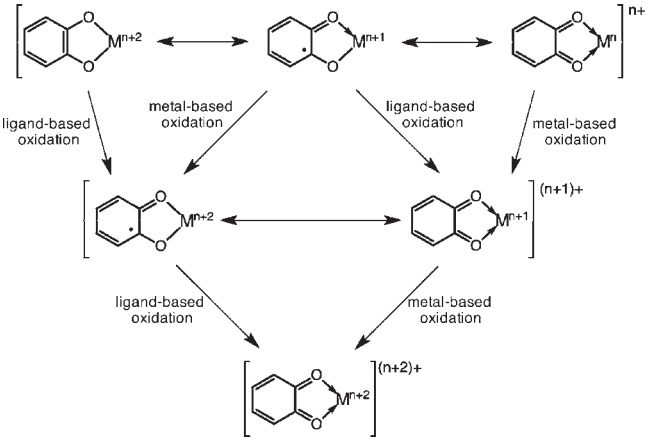

these metals would be attractive because it would open up a new class of atom- and group-transfer catalysts.

Redox-Active Ligands. Redox-active ligands can exist in multiple oxidation states when coordinated to a transition metal.[20−24] Catecholate is the prototypical redox-active ligand, with three potential oxidation states: the dianionic catecholate, the monoanionic open-shell radical semiquinonate, and the neutral quinone. Upon coordination of catecholate-type ligands to transition metals, even a cursory assignment of the metal oxidation state becomes a challenging problem for both experiment and theory.[25,26] Chart 2 summarizes the electronic complexity arising from the coordination of a redox-active ligand to a redox-active metal. As shown across the top of Chart 2, resonance structures can be drawn that change the distribution of electrons between the redox-active ligand and the coordinated metal without changing the total number of valence electrons contained within the two fragments. In complexes with strong metal−ligand π interactions, these resonance structures help to describe the complicated electronic interactions between closely matched metal and ligand frontier orbitals within the simple Lewis formalism. In some complexes, the different electron distributions illustrated across the top of Chart 2 are better described as electronic isomers (connected by equilibrium arrows) because the electron distributions represent different local minima on the potential energy surface.[21,27,28]

Moving vertically in Chart 2 represents redox transformations within the metal−ligand fragment that change the total number of valence electrons contained within the unit. In classic transition-metal coordination chemistry, redox changes are considered to occur mainly within the d-orbital manifold, so removing an electron from a coordination complex results in an increase in the metal oxidation state (metal-based oxidations). In complexes with redox-active ligands, removal of an electron from the complex can increase the oxidation level of the ligand (ligand-based oxidation), leaving the metal oxidation state unchanged. As illustrated in Chart 2, these two limiting processes give species with the same number of valence electrons within the metal−ligand unit. With strong metal−ligand π interactions, these species again are best described as limiting resonance structures. For the removal of a second electron from the metal−ligand fragment, it does not matter if the electron comes from the ligand or from the metal because only a single resonance structure and electron distribution is possible.

The implication of the simple model provided in Chart 2 is that, for coordination complexes with strongly interacting metal and ligand frontier orbitals, the metal and redox-active ligand can work together to accommodate valence changes associated with a redox reaction.[29] Mapping this concept onto the zirconium−imide bond-activation chemistry of Chart 1 suggests that redox-active ligands may provide a mechanism for realizing formal nitrene-transfer reactivity. Thus, a zirconium imido complex that also contains a redox-active ligand might perform an initial substrate activation step such as [2 + 2] cycloaddition or C−H bond activation and follow it up with a two-electron, C−N bond-forming reductive elimination to afford an aziridine or an amine, respectively. The reductive elimination step would be made possible because the redox-active ligand can accept two electrons, circumventing the formation of a high-energy zirconium(II) species. Adding a suitable nitrene-transfer reagent might then close a catalytic cycle for olefin aziridination or C−H bond amination.

II. LIGAND DESIGN

In order to develop the type of metal−ligand cooperative redox reactivity hinted at in Chart 2, redox-active ligands are needed with frontier orbitals that energetically match the early-transition-metal d orbitals. The ligands also need to provide a coordination environment that secures these reactive ions. Earlier work from our laboratory on zirconium complexes of *o*-phenylenediamine[30] and *o*-aminophenol[31,32] derivatives showed that these catecholate-type ligands provide the desired electronic matching of ligand and metal orbitals to achieve both oxidative addition and reductive elimination reactivity (Scheme 1). It became readily apparent that a common problem associated with the use of bidentate redox-active ligands with d^0 early-transition-metal ions was the stability of the metal coordination environment. Namely, while catecholate complexes of d^0 metals can show incredible formation constants and stability,[33] upon oxidation of amidophenolate ligands to the semiquinonate or quinone oxidation states, ligand dissociation can be quite fast. For example, the bis(amidophenolate) complex, $[ap]_2Zr(THF)_2$ (ap^{2-} = 4,6-di-*tert*-butyl-2-*tert*-butylamidophenolate; THF = tetrahydrofuran) is stable to dissociation of the redox-active amidophenolate ligand; however, upon two-electron oxidation to $[isq]_2ZrCl_2$ (isq^- = 4,6-di-*tert*-butyl-2-*tert*-butyliminosemiquinonate),[34] the complex is unstable over long periods in solution, and ligand exchange occurs to form $[isq]_4Zr$ complexes. When $[ap]_2Zr(THF)_2$ is

dx.doi.org/10.1021/ic200911b |*Inorg. Chem.* 2011, 50, 9849–9863

Scheme 1

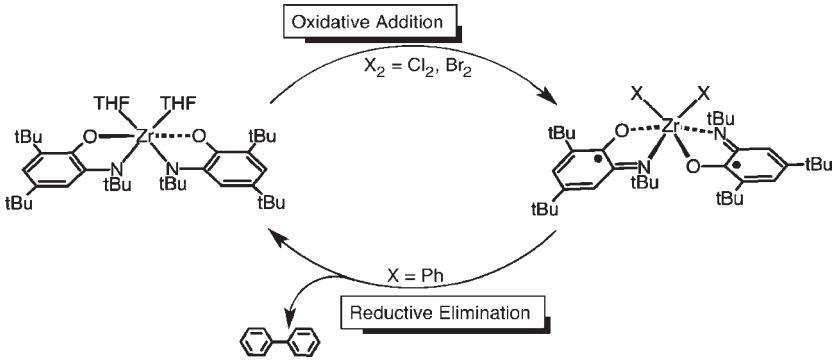

Chart 3

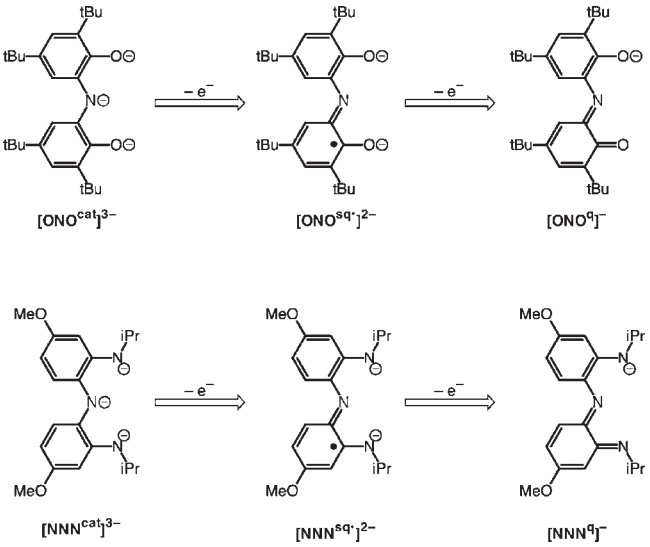

oxidized by four electrons, iminoquinone is immediately ejected from the metal coordination sphere.

To combat the dissociation of oxidized semiquinonate and quinone ligands from the coordination spheres of d^0 metal complexes, we sought redox-active ligands with higher denticities. While the initial results with a tetradentate ligand derived by condensing 2 equiv of 3,5-di-*tert*-butylcatechol with 1 equiv of *o*-phenylenediamine were promising,[35,36] the planar ligand topology and tetraanionic charge (in its fully reduced form) made elaboration of the ligand platform challenging. Furthermore, despite the incorporation of three catecholate-type rings into the macrocyclic structure, the ligand could only be oxidized twice, with the oxidation localized in the unprotected central phenylenediamide fragment.

The so-called pincer-ligand family provides an alternative topology for a redox-active ligand.[37,38] A redox-active pincer ligand can be prepared by stitching together two catechols through condensation with ammonia. The *in situ* reaction of 3,5-di-*tert*-butylcatechol and ammonia in the presence of MX_2 salts (e.g., M = Fe, Mn, Cu, and Zn) and air afforded $M[ONO]_2$ complexes with octahedral geometries enforced by the meridional coordination of two tridentate amidobis(phenolates).[39,40] The redox-activity of the ligands was evident because all of the complexes were isolated as neutral species with complicated electronic and magnetic properties. The three common oxidation states of the [ONO] ligand are shown in Chart 3. In the fully reduced or catecholate form, $[ONO^{cat}]^{3-}$, the ligand is closed-shell and formally trianionic. Removal of one electron affords an open-shell radical semiquinonate that is formally dianionic, $[ONO^{sq}]^{2-}$. Removal of a second electron returns the ligand to a closed-shell configuration as the monoanionic, quinonate form of the ligand, $[ONO^{q}]^{-}$. The ligand typically coordinates to metal ions in a meridional fashion, and this planar geometry within the ligand allows for delocalization of the valence electronic changes over both six-membered rings. A synthetic route for preparing and isolating the tridentate ligand in its "apo" form, $[ONO^{cat}]H_3$, has been reported,[41] and the [ONO] platform has been used as a noninnocent ligand in the preparation of copper oxidation catalysts for alcohol oxidation[41] and as a supporting ligand in the preparation of valence-tautomeric complexes.[21]

A redox-active pincer ligand analogous to the [ONO] platform but with an all-nitrogen donor set is another attractive target. The replacement of the oxygen donors of [ONO] with nitrogen donors provides both different electronic properties and tunable steric properties. An Ullman coupling between 2-nitroanisidine and 3-iodo-4-nitroanisole followed by Zn/HOAc reduction affords the backbone for an all-nitrogen redox-active ligand, $[NNN^{cat}]H_3$.[42] Treatment of the triammine with acetone and $NaBH_3CN$ results in the installation of isopropyl groups onto the primary amines via a reductive condensation. Trimethylsilyl[43] and amide[44] derivatives also have been reported, but the redox properties of these derivatives have not been thoroughly developed. Three oxidation states of the [NNN] ligand platform are shown alongside those of the [ONO] ligand in Chart 3.

This manuscript provides an overview of our recent efforts to utilize [ONO] and [NNN] redox-active, pincer-type ligands for multielectron reactivity at electrophilic d^0 metal centers. New and previously reported[42,45,46] results are discussed within the context of developing nitrene-transfer reactivity for group IV and V metal complexes. First, the electronic properties engendered by the [ONO] and [NNN] ligand platforms are examined, with consideration given to redox potentials, redox reactivity, and spectroscopic interrogations of valence-electron distributions between the redox-active ligand and coordinated metal ion. Second, two-electron nitrene-group-transfer chemistry to tantalum(V) and zirconium(VI) complexes of the $[NNN^{cat}]^{3-}$ ligand is discussed, highlighting the importance of the metal coordination environment in the formation of monomeric and

dx.doi.org/10.1021/ic200911b |*Inorg. Chem.* 2011, 50, 9849–9863

Scheme 2

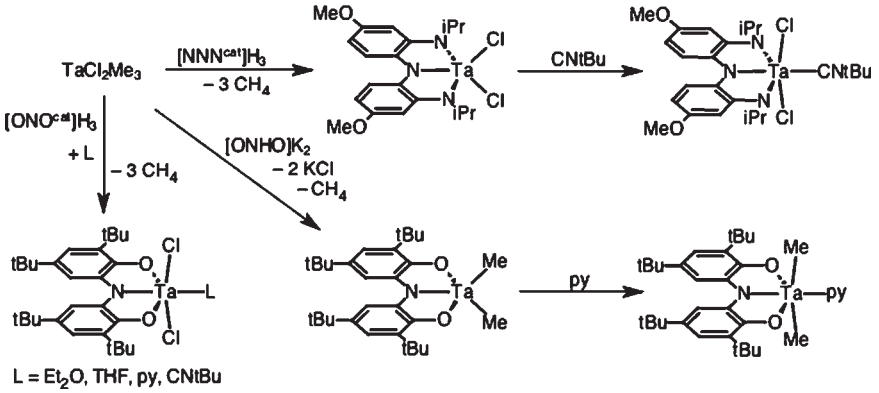

dimeric metal imide complexes and the subsequent reactivity of the metal imide functionality. Third, the nitrene reactivity of [ONO] complexes of tantalum(V) is discussed. These complexes show a strong proclivity for mediating N−N bond formation. The paper concludes with an outlook speculating on the further development of multielectron and group-transfer chemistry using early transition metals and redox-active ligands.

III. BENCHMARKING REDOX-ACTIVE LIGAND PROPERTIES

The $[ONO^{cat}]H_3$ and $[NNN^{cat}]H_3$ ligands are readily coordinated to tantalum through the use of the mixed methyl chloride tantalum synthon $TaCl_2Me_3$, as summarized in Scheme 2.[42,46] The triprotic $[NNN^{cat}]H_3$ ligand is acidic enough to react with all three methyl groups of $TaCl_2Me_3$ to release methane and afford the five-coordinate complex $[NNN^{cat}]TaCl_2$ in good yield. Similarly, the $[NNN^{cat}]H_3$ ligand reacts rapidly with $TaCl_2Me_3$ to release methane; however, in this case the isolated tantalum complex is a six-coordinate Lewis basic adduct, $[ONO^{cat}]$-$TaCl_2L$, with a coordinated diethyl ether, THF, or pyridine ligand. The [ONO]Ta unit also may be accessed by taking advantage of the different pK_a's associated with the phenolic and diphenylamine protons of $[ONO^{cat}]H_3$. Hence, deprotonation of $[ONO^{cat}]H_3$ with 2 equiv of KH to generate the putative $[ONHO]K_2$, followed by the addition of $TaCl_2Me_3$, afforded the dimethyl complex $[ONO^{cat}]TaMe_2$. The dimethyl complex could be isolated as the five-coordinate, base-free species owing to the strong electron-donating properties of the two methyl ligands; however, in the presence of a strong Lewis base like pyridine, the six-coordinate $[ONO^{cat}]TaMe_2(py)$ adduct was obtained.

Isocyanide adducts of $[ONO^{cat}]TaCl_2$ and $[NNN^{cat}]TaCl_2$ were prepared so that vibrational spectroscopy could be used as a probe of the electron-donating nature of the two redox-active ligands. Treatment of $[ONO^{cat}]TaCl_2(OEt_2)$ with 1 equiv of *tert*-butylisocyanide led to ligand substitution and formation of the adduct $[ONO^{cat}]TaCl_2(CNtBu)$. While $[NNN^{cat}]TaCl_2$ was isolated as the base-free five-coordinate complex, it reacted quantitatively with the isocyanide to afford the analogous adduct $[NNN^{cat}]TaCl_2(CNtBu)$.[42] In both complexes, the isocyanide ligand coordinated trans to the nitrogen donor of the redox-active ligand to afford C_{2v}-symmetric species. The IR spectra of $[ONO^{cat}]TaCl_2(CNtBu)$ and $[NNN^{cat}]TaCl_2(CNtBu)$ were recorded as KBr pellets with C≡N vibrations observed at 2225 and 2203 cm^{-1}, respectively. Both of these vibrational frequencies are blue-shifted relative to the C≡N vibration for free *tert*-butylisocyanide (2125 cm^{-1}), consistent with coordination of the ligand to a d^0 metal;[47] however, the smaller blue shift of the isocyanide vibrational frequency in $[NNN^{cat}]TaCl_2(CNtBu)$ is consistent with a less electron-poor tantalum center in the [NNN] derivative. For further comparison, the C≡N vibration of the 16-electron tantalum(V) complex $Cp^*TaCl_4(CNtBu)$ was observed at 2241 cm^{-1},[48] while the C≡N vibrations of the 18-electron tantalum cations $[(C_5H_4tBu)_2Ta^V(H)_2(CNtBu)]^+$ and $[Cp_2Ta^{III}(H_2C{=}CHR)(CNtBu)]^+$ were observed at 2210 and 2164 cm^{-1}, respectively.[49,50] These comparisons suggest that $[ONO^{cat}]^{3-}$ and $[NNN^{cat}]^{3-}$ ligands are strongly electron-donating toward the tantalum center, without formally reducing the metal to the Ta^{III} oxidation state. Consistent with this hypothesis, attempts to make the analogous CO complexes, $[ONO^{cat}]TaCl_2(CO)$ and $[NNN^{cat}]TaCl_2(CO)$, were unsuccessful, providing further qualitative evidence that the tantalum metal center is not in a highly reduced formal oxidation state (i.e., Ta^{III}).

The redox reactivity of $[ONO^{cat}]TaCl_2L$ was benchmarked using halogen oxidation reactions. The chlorine surrogate $PhICl_2$ afforded $[ONO^{sq}]TaCl_3$ and $[ONO^{q}]TaCl_4$ upon one- and two-electron oxidation of $[ONO^{cat}]TaCl_2(OEt_2)$, respectively, as shown in Scheme 3.[46] The one-electron oxidation product, $[ONO^{sq}]TaCl_3$, is a paramagnetic, $S = {}^1/_2$, complex, while the two-electron oxidation product, $[ONO^{q}]TaCl_4$, is a diamagnetic complex. The reaction progress is readily indicated by color changes from red to blue to green as the [ONO] ligand is oxidized from the catecholate to the semiquinonate to the quinonate form.

Single-crystal X-ray diffraction studies provide unequivocal data on the experimental metal and ligand oxidation states for $[ONO^{cat}]TaCl_2(OEt_2)$, $[ONO^{sq}]TaCl_3$, and $[ONO^{q}]TaCl_4$. Table 1 shows selected bond lengths for these three complexes. Of note are the $Ta-Cl_{ax}$ bond distances (those perpendicular to the [ONO]Ta plane), which fall in the 2.34−2.38 Å range across the redox series. These distances are typical of chloride bond distances in other tantalum(V) complexes. Ta−Cl bond distances within the same plane as the [ONO] ligand show greater variability owing to steric crowding that occurs in the seven-coordinate $[ONO^{q}]TaCl_4$ complex. Bond distances between the tantalum center and the [ONO] ligand increase upon going from $[ONO^{cat}]TaCl_2(OEt_2)$ to $[ONO^{sq}]TaCl_3$ to $[ONO^{q}]TaCl_4$, consistent with oxidation of the [ONO] ligand across the series.

dx.doi.org/10.1021/ic200911b |*Inorg. Chem.* 2011, 50, 9849–9863

Scheme 3

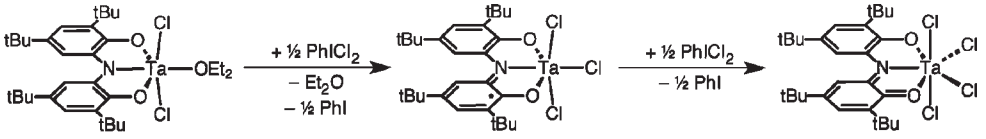

Table 1. Comparison of Selected Bond Distances (Å) in the Ligand Oxidation Series $[ONO^{cat}]TaCl_2(OEt_2)$, $[ONO^{sq}]TaCl_3$, and $[ONO^{q}]TaCl_4$[c]

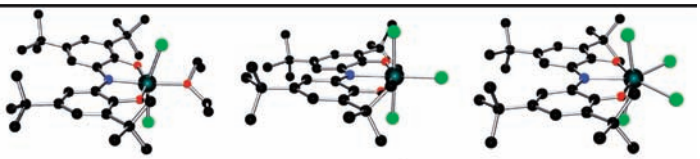

	$[ONO^{cat}]TaCl_2(OEt_2)$[a]	$[ONO^{sq}]TaCl_3$[b]	$[ONO^{q}]TaCl_4$[b]
Ta–Cl_{ax} (avg)	2.377(3) Å	2.3686(14) Å	2.3436(11) Å
Ta–Cl_{eq} (avg)	--	2.312(5) Å	3.4138(13) Å
Ta–O (avg)	1.876(6) Å	1.915(4) Å	2.016(3) Å
Ta–N	2.043(7) Å	2.222(5) Å	2.362(3) Å
O–C (avg)	1.390(11) Å	1.342(7) Å	1.300(5) Å
N–C (avg)	1.410(13) Å	1.362(7) Å	1.349(5) Å

[a] This work. [b] See ref 46. [c] The equatorial plane is defined by the tantalum and the [ONO] ligand.

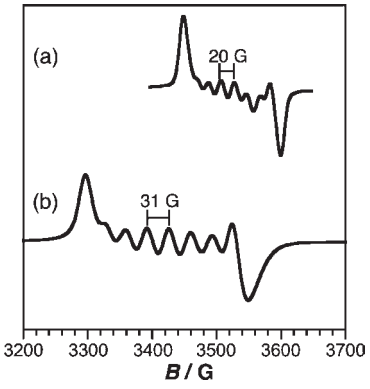

Figure 1. X-band solution EPR spectra of (a) $[ONO^{sq}]TaCl_3$ and (b) $[NNN^{sq}]TaCl_3$ collected at 298 K in THF. The spectra give g = 1.979 for $[ONO^{sq}]TaCl_3$ and g = 1.897 for $[NNN^{sq}]TaCl_3$.

Congruous with this interpretation is the trend in the O−C and N−C bond distances within the [ONO] ligand, which contract as the ligand is oxidized.

In contrast to the reactivity of $[ONO^{cat}]TaCl_2(OEt_2)$, the reaction of $[NNN^{cat}]TaCl_2$ with $PhICl_2$ affords only the single-electron oxidation product $[NNN^{sq}]TaCl_3$ with no evidence for the formation of $[NNN^{q}]TaCl_4$.[42] The one-electron-oxidized $[NNN^{sq}]TaCl_3$ product is a paramagnetic species that was characterized by electron paramagnetic resonance (EPR) spectroscopy. Figure 1 shows the X-band solution EPR spectra of both $[ONO^{sq}]TaCl_3$ and $[NNN^{sq}]TaCl_3$ at 298 K. Both spectra show isotropic room-temperature signals consistent with $S = {}^1/_2$ spin systems and hyperfine coupling to $I = {}^7/_2$ tantalum nuclei. The larger isotropic hyperfine coupling constant, A_{iso}, of 31 G in $[NNN^{sq}]TaCl_3$ is suggestive of greater delocalization of the unpaired electron onto the tantalum center than in the $[ONO^{sq}]TaCl_3$ complex (A_{iso} = 20 G); however, both of these values are smaller than those observed for organometallic tantalum(IV) complexes (A_{iso} = 61−113 G)[51] and for the tantalum(IV) coordination complex $TaCl_4(PEt_3)_2$ (A_{iso} = 211 G).[52] Given prior literature indicating that redox-active ligands derived from *o*-phenylenediamine are easier to oxidize than those derived from catechol or *o*-aminophenol,[53] the inaccessibility of the two-electron oxidation product, putative $[NNN^{q}]TaCl_4$, was surprising. To gain insight into whether this result was a consequence of steric or electronic differences between the [ONO] and [NNN] ligands, the two platforms were examined electrochemically.

To probe the ligand redox properties, the six-coordinate $[ONO^{sq}]TaCl_3$ and $[NNN^{sq}]TaCl_3$ complexes were investigated by cyclic voltammetry. Figure 2 shows the cyclic voltammetry data for both complexes collected in CH_2Cl_2 using a platinum disk electrode and a 0.1 M $[Bu_4N][PF_6]$ electrolyte. All potentials are referenced to $[Cp_2Fe]^{+/0}$. $[ONO^{sq}]TaCl_3$ shows a reversible ($i_{pa} \cong i_{pc}$) one-electron reduction at −0.12 V and a partially reversible ($i_{pa} < i_{pc}$) oxidation at +0.48 V. The $[NNN^{sq}]TaCl_3$ analogue shows a reversible one-electron reduction at −0.32 V and a reversible one-electron oxidation at +0.15 V. Two points about this data are worth emphasizing. First, the electrochemical measurements clearly establish that the [NNN] ligand platform is, in fact, easier to oxidize than the [ONO] ligand platform. The oxidation from catecholate to semiquinonate is 200 mV easier for the [NNN] platform than it is for the [ONO] platform; the oxidation from semiquinonate to quinonate is 300 mV easier for the [NNN] platform than it is for the

dx.doi.org/10.1021/ic200911b |*Inorg. Chem.* 2011, 50, 9849–9863

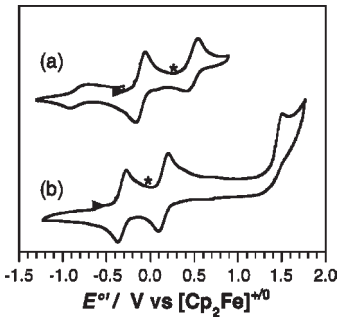

Figure 2. Cyclic voltammograms of (a) $[ONO^{sq}]TaCl_3$ and (b) $[NNN^{sq}]TaCl_3$ in CH_2Cl_2 with 0.1 M $[Bu_4N][PF_6]$ at 200 mV s^{-1}. The stars (★) denote the potentials of the bulk tantalum complex. Potentials are referenced to $[Cp_2Fe]^{+/0}$.

[ONO] platform. Second, the semiquinone-to-quinone oxidation of the [NNN]Ta species is more reversible than the corresponding oxidation of the [ONO]Ta species. We attribute this difference in reversibility to differences in the steric constraints imposed by the [ONO] and [NNN] platforms. Oxidation of $[ONO^{sq}]TaCl_3$ to $[ONO^{q}]TaCl_3^+$ generates an electrophilic and reactive cation. As illustrated by the crystal structure of $[ONO^{q}]TaCl_4$, the [ONO] ligand platform can accommodate a seven-coordinate geometry at tantalum. In the electrochemical experiment, the $[ONO^{q}]TaCl_3^+$ cation likely adds whatever ligand it can find in solution (for example, by binding a $[PF_6]^-$ anion),[54−56] leading to irreversibility in the $[ONO^{sq}]TaCl_3$ to $[ONO^{q}]TaCl_3^+$ redox process (EC reaction). In contrast, the increased steric constraints imposed by the *i*Pr groups of the [NNN] ligand disfavor seven-coordinate geometries at tantalum and prevent the coordination of Lewis bases to the electrophilic tantalum center of $[NNN^{q}]TaCl_3^+$; therefore, on the electrochemical time scale, the $[NNN^{sq}]TaCl_3$ to $[NNN^{q}]TaCl_3^+$ redox process is reversible.

Combining the electrochemical results presented in Figure 2 with the halogen reactivity of $[ONO^{cat}]TaCl_2L$ and $[NNN^{cat}]$-$TaCl_2$ provides insight into the factors governing the reactivity of these two platforms. In the case of the [ONO] ligand, the two-electron oxidation product, $[ONO^{q}]TaCl_4$, is an isolable complex thanks to the stabilization provided by coordination of the fourth halide to the tantalum center. In the case of the [NNN] ligand, the first chlorine atom addition to $[NNN^{cat}]TaCl_2$ gives six-coordinate $[NNN^{sq}]TaCl_3$. The addition of the second chlorine atom should (and probably does) oxidize the [NNN] ligand up to the quinone oxidation state; however, the N(*i*Pr) groups block access to a seven-coordinate structure and, hence, coordination of the fourth chloride ligand. While the putative $[NNN^{q}]TaCl_3^+$ cation is stable on the electrochemical time scale, it may not be stable enough to allow for isolation (repeated attempts to isolate this species with a variety of noncoordinating anions failed); a possible decomposition pathway may involve hydrogen-atom abstraction from the methine carbon of a N(*i*Pr) group.

Two key observations can be made regarding the reactivity patterns of the [ONO]Ta and [NNN]Ta platforms: the first an electronic effect and the second a steric effect. First, vibrational spectroscopy and electrochemical analyses both suggest that the [NNN] redox-active ligand provides a more reducing environment for the coordinated metal than the oxygen derivative [ONO] redox-active ligand. While the electrochemical data

Scheme 4

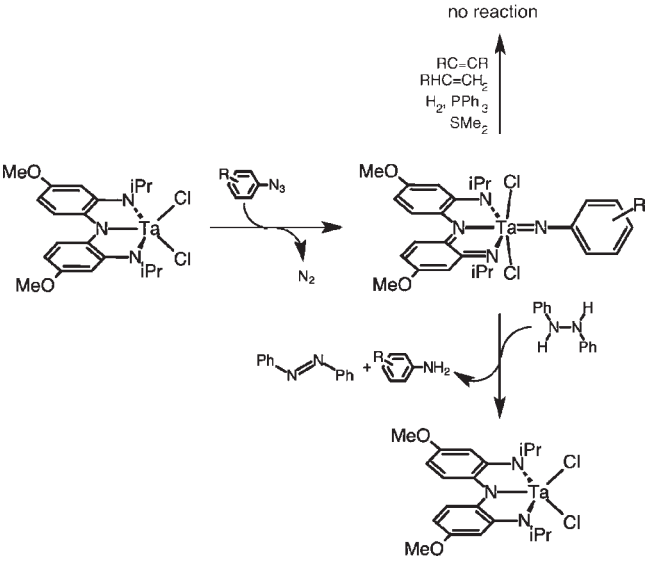

suggest that both ligand platforms can access the catecholate, semiquinonate, and quinonate oxidation states, the potentials for the [NNN] redox-active ligand are 200−300 mV lower than those for the [ONO] redox-active ligand. Second, despite this clear evidence that the [NNN] ligand is easier to oxidize than the [ONO] derivative, chemical oxidations using chlorine surrogates indicate that sterics play a big part in stabilizing the oxidation products. Given these results, it seemed plausible that two-electron reactivity would be possible for the [NNN]Ta platform, provided that seven-coordinate species could be avoided.

IV. NITRENE-TRANSFER REACTIVITY OF $[NNN^{cat}]TaCl_2$

On the basis of the identification of two reversible one-electron redox processes for the [NNN]Ta platform, we sought to develop two-electron group-transfer reactivity. According to Scheme 4, the treatment of $[NNN^{cat}]TaCl_2$ with aryl azides resulted in liberation of N_2 and concomitant formation of the tantalum imide complex $[NNN^{q}]TaCl_2(=NAr)$ (Ar = Ph, *p*-tolyl, 4-C_6H_4tBu, 3,5-$C_6H_3Me_2$).[42] Azides with more sterically demanding aryl substituents (i.e., 2,6-C_6H_3iPr$_2$) did not react with $[NNN^{cat}]TaCl_2$ nor did alkyl azides or trimethylsilyl azide. Similarly, the Lewis-base adduct $[NNN^{cat}]TaCl_2$(py) did not react with aryl azides, highlighting the importance of an open coordination site at the metal center. Figure 3 shows the structure of $[NNN^{q}]TaCl_2(=NPh)$ along with pertinent bond distances within the metal coordination sphere and the [NNN] ligand. The Ta−N and Ta−Cl bond distances are typical for a tantalum(V) complex. The bond distance for the tantalum imide is consistent with the triple-bond character between a d^0 tantalum center and an imide ligand acting as a six-electron donor.[12,57−59] Consistent with this contention is the Ta−N−C bond angle within the imide, which is close to linear at 167.4(4)°. Within the [NNN] ligand, the bond distances clearly indicate the quinone oxidation state, with the pattern of C−C bond distances consistent with cyclohexadiene rings.[60]

The imide in $[NNN^{q}]TaCl_2(=NAr)$ can be reduced with hydrazine, but attempts to react it with other organic substrates have been unsuccessful. $[NNN^{q}]TaCl_2(=NPh)$ reacts cleanly

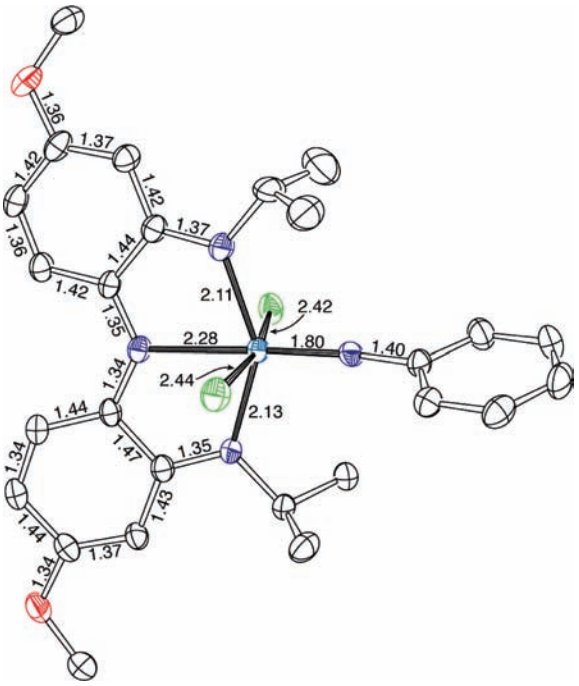

Figure 3. ORTEP diagram of [NNN^{q}]TaCl$_2$(=NPh). Thermal ellipsoids are shown at 50% probability, and hydrogen atoms are omitted for clarity. Bond distances are given in angstroms to the hundredths decimal place. Data were taken from a high-resolution structure in which the errors in the C−O,N,C distances were <0.01 Å.[42]

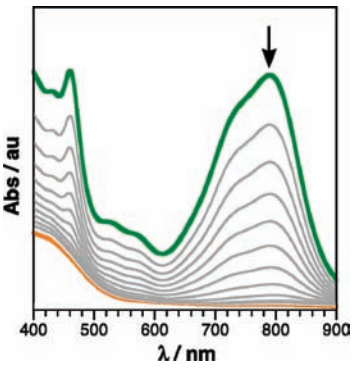

Figure 4. Changes in the electronic absorption spectrum during the reaction of [NNN^{q}]TaCl$_2$(=NPh) with excess 1,2-diphenylhydrazine in THF. Spectra were recorded in 30 min intervals at 35 °C.

with 1,2-diphenylhydrazine to afford aniline and azobenze according to Scheme 4. When the reaction was carried out in THF at room temperature, there was no evidence for the buildup of an intermediate species such as [NNN^{sq}]TaCl$_2$(NHPh), which would be expected to have a distinctive absorption in the visible portion of the spectrum. Instead, the spectrum for the imido complex [NNN^{q}]TaCl$_2$(=NPh) cleanly decays to the spectrum of the fully reduced [NNN^{cat}]TaCl$_2$ (Figure 4). Reactions carried out using [NNN^{q}]TaCl$_2$(=N-4-C$_6$H$_4$*t*Bu) and 1,2-diphenylhydrazine yielded the exclusive formation of *p*-*tert*-butylaniline and azobenzene, indicating an hydrogen-atom-transfer or a proton-coupled electron-transfer pathway[61,62] rather than a metathesis pathway involving cleavage of the N−N bond of the hydrazine reductant. Reactions with other potential

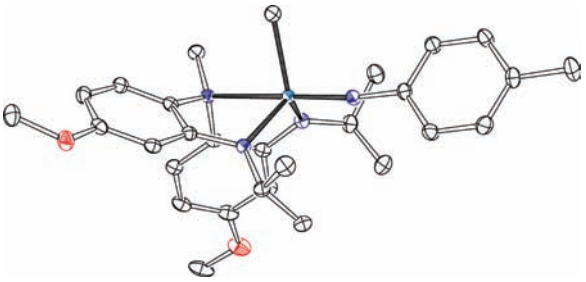

Figure 5. ORTEP diagram of [NN(Me)N]TaMe(=N-*p*-tolyl). Thermal ellipsoids are shown at 50% probability, and hydrogen atoms are omitted for clarity.

hydrogen-atom donors such as 9,10-dihydroanthracene or 1,4-cyclohexadiene did not result in reduction of the imido complex, nor did any [NNN^{q}]TaCl$_2$(=NAr) react with H$_2$ or the C−H bonds of benzene, toluene, or other alkanes. Attempts to transfer the nitrene to unsaturated organic substrates such as α-olefins and alkynes were unsuccessful. These results suggest that while [NNN^{q}]TaCl$_2$(=NAr) is susceptible to proton-coupled electron-transfer reactivity, it is not capable of two-electron nitrene-transfer chemistry analogous to mid- and late-transition-metal imido complexes.

Attempts to generate organometallic tantalum imide complexes resulted in alkylation of the [NNN] ligand.[63] The addition of 2 equiv of MeLi to solutions of [NNN^{q}]TaCl$_2$(=NAr) complexes led to N-methylation of the redox-active ligand and formation of [NN(Me)N]TaMe(=NAr). Single crystals of one derivative, [NN(Me)N]TaMe(=N-*p*-tolyl), were obtained and provided the molecular structure shown in Figure 5. Methylation of the ligand is readily apparent in the structure and results in the [NN(Me)N] ligand adopting more of a facial coordination mode (N−Ta−N 114°). The Ta−N distance to the methylated nitrogen is long at 2.38 Å, consistent with this nitrogen acting as a neutral amine donor. The Ta−N distance to the imide ligand remains short at 1.80 Å, and the Ta−N−C bond angle is opened further (173°) relative to [NNN^{q}]TaCl$_2$(=NPh). The ^{1}H and ^{13}C NMR spectra of [NN(Me)N]TaMe(=N-*p*-tolyl) are entirely consistent with the X-ray structure. The resonance for the [NN(Me)N] methyl group appears as a singlet at 3.03 ppm in the ^{1}H NMR spectrum and the tantalum-bound methyl appears at 0.83 ppm. Reactions between [NNN^{q}]TaCl$_2$(=NAr) and 1 equiv of MeLi did not proceed as cleanly as those with 2 equiv of MeLi; however, according to NMR spectroscopy, the primary product of those reactions is the ligand-methylated species, [NN(Me)N]TaCl(=NAr). This result suggests that the initial reaction between [NNN^{q}]TaCl$_2$(=NAr) and MeLi is nucleophilic attack of Me^{-} at the quinonate ligand, a contention that is supported by the observed geometry in the [NN(Me)N]-TaMe(=N-*p*-tolyl) product.

We surmised that a potential problem with utilizing [NNN^{q}]TaCl$_2$(=NAr) as a platform for nitrene transfer to substrates was coordinative saturation at the tantalum metal center. [NNN^{q}]TaCl$_2$(=NAr) is a six-coordinate, 16-electron complex. The N(*i*Pr) groups of the [NNN] ligand effectively block access to the metal center, preventing coordination of a substrate that can accept the nitrene. In order to examine the reactivity of the imido fragment with reductants other than hydrazines, it would be necessary to open a coordination site at the metal center. Attempts to abstract a chloride ligand from

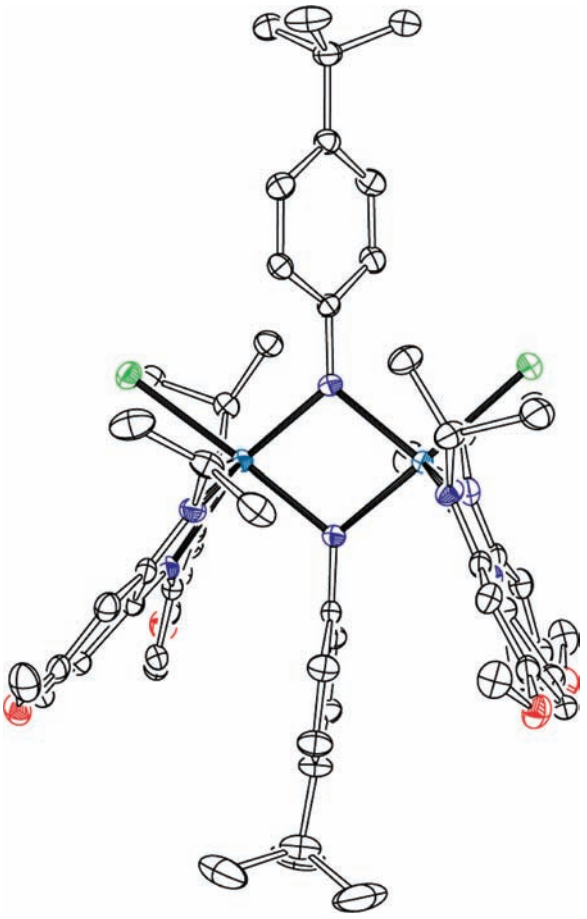

Figure 6. ORTEP diagram of $\{[NNN^{q}]ZrCl(\mu^{2}\text{-N-4-}C_6H_4t\text{Bu})\}_2$.[45] Thermal ellipsoids are shown at 50% probability. Hydrogen atoms and a diethyl ether solvent molecule are omitted for clarity.

$[NNN^{q}]TaCl_2(=NAr)$ with various boranes and alumanes did not afford the desired five-coordinate $[NNN^{q}]TaCl(=NAr)^{+}$ cation. As an alternative method to generating a five-coordinate imido complex, analogous [NNN] complexes of zirconium were prepared.

V. CATALYTIC NITRENE TRANSFER BY $[NNN^{cat}]ZrCl(CNtBu)_2$[45]

Coordination of the [NNN] ligand platform to zirconium affords a six-coordination, pseudooctahedral complex, $[NNN^{cat}]ZrCl(THF)_2$. Metalation was readily achieved by treating $ZrCl_4(THF)_2$ with the deprotonated ligand, $[NNN^{cat}]Li_3(OEt_2)_n$ (formed *in situ*), in diethyl ether. While the product, $[NNN^{cat}]ZrCl(THF)_2$, is a saturated six-coordinate complex, two of the coordination sites are taken up by substitutionally labile THF ligands. Indeed, the ^{1}H NMR spectrum of $[NNN^{cat}]ZrCl(THF)_2$ in the presence of free THF shows only a single set of THF resonances at room temperature, consistent with rapid exchange between free and coordinated THF on the NMR time scale. The THF ligands are readily displaced by more strongly donating ligands, and as such the addition of 2 equiv of pyridine or *tert*-butylisocyanide to $[NNN^{cat}]ZrCl(THF)_2$ resulted in the quantitative formation of $[NNN^{cat}]ZrCl(py)_2$ or $[NNN^{cat}]ZrCl(CNtBu)_2$, respectively. In all three complexes, the NMR spectra show C_{2v}-symmetric species, suggesting that the chloride ligand is coordinated trans to the central nitrogen of the [NNN] ligand. As with the analogous tantalum complex, $[NNN^{cat}]TaCl_2(CNtBu)$, the zirconium derivative $[NNN^{cat}]ZrCl(CNtBu)_2$ shows the C≡N stretch to higher frequency (2201 cm^{-1}) than the C≡N stretch in free isocyanide (2125 cm^{-1}), consistent with an electron-poor metal center.

Aryl azides react with $[NNN^{cat}]ZrCl(THF)_2$, transferring the nitrene to the metal center and yielding a dimeric zirconium imide complex. Conversion of $[NNN^{cat}]ZrCl(THF)_2$ to the oxidized imido dimer $\{[NNN^{q}]ZrCl(\mu\text{-NAr})\}_2$ (Ar = Ph, 4-C_6H_4tBu, *p*-tolyl, 4-$C_6H_4CF_3$, 2,4,6-$C_6H_2Me_3$) was readily monitored by optical spectroscopy as the orange starting material gives way to an olive-green product with an intense absorption band at ~430 nm. While the complexes show overall C_{2v} symmetry by NMR spectroscopy, two inequivalent imido ligands are evident. X-ray-quality crystals of the 4-*tert*-butylphenylimido derivative were obtained, and the structure is shown as an ORTEP diagram in Figure 6. The zirconium dimer forms with the chloride ligands occupying syn positions with respect to the Zr···Zr vector, an arrangement that forces the two [NNN] ligands to sandwich one bridging imide ligand. As with the monomeric tantalum analogue, the bond lengths within the [NNN] ligand indicate that both ligands are in the quinonate oxidation state.

Despite the chemically distinct environments of the two bridging imido ligands in the $\{[NNN^{q}]ZrCl(\mu\text{-NAr})\}_2$ complexes, they proved to be unreactive. Heating mixtures of $\{[NNN^{q}]ZrCl(\mu\text{-NPh})\}_2$ and $\{[NNN^{q}]ZrCl(\mu\text{-N-}p\text{-tolyl})\}_2$ for days in benzene did not lead to crossover formation of the putative mixed imido complex $\{[NNN^{q}]ZrCl\}_2(\mu\text{-NPh})(\mu\text{-N-}p\text{-tolyl})$. Similarly, olefins, alkynes, phosphines, sulfides, and isocyanides failed to react with the imido dimers under thermal conditions. Presumably, the aryl azides react with $[NNN^{cat}]ZrCl(THF)_2$ to form a terminal imido complex initially, $[NNN^{q}]ZrCl(=NAr)(THF)$, which then loses THF and dimerizes to form the observed product. The unreactive nature of this dimeric complex under thermal conditions indicates that formation of the bridging imide core is not reversible under thermally accessible conditions; thus, any transfer of the nitrene from the metal center to a substrate must occur prior to dimerization of the putative terminal imide intermediate.

The bis(isocyanide) complex, $[NNN^{cat}]ZrCl(CNtBu)_2$, offered a way to intercept a putative terminal zirconium imide intermediate. The treatment of $[NNN^{cat}]ZrCl(CNtBu)_2$ with 1 equiv of 4-$tBuC_6H_4N_3$ resulted in liberation of 1 equiv of N_2 gas and formation of the carbodiimide 4-$tBuC_6H_4N{=}C{=}NtBu$.[64,65] The remaining zirconium complex was characterized by the addition of pyridine to the solution upon completion of the reaction and gave quantitative recovery of $[NNN^{cat}]ZrCl(py)_2$. In the presence of excess aryl azide and excess *t*BuNC, up to 2 equiv of carbodiimide was formed per zirconium complex. When the alkyl azides $tBuN_3$ or AdN_3 were used in excess with excess *t*BuNC, the catalytic formation of carbodiimide was observed corresponding to approximately 10 turnovers of the zirconium complex. Attempts to run the nitrene-transfer reaction with lower catalyst loadings were unsuccessful because the reaction is impeded both by isocyanide and by the carbodiimide product. Replacement of isocyanide with CO resulted in no nitrene transfer to form isocyanate. A simplified mechanism for the nitrene-transfer reaction that takes into account these observations is shown in Scheme 5. The inverse dependence of the reaction rate on the isocyanide concentration suggests that the

Scheme 5

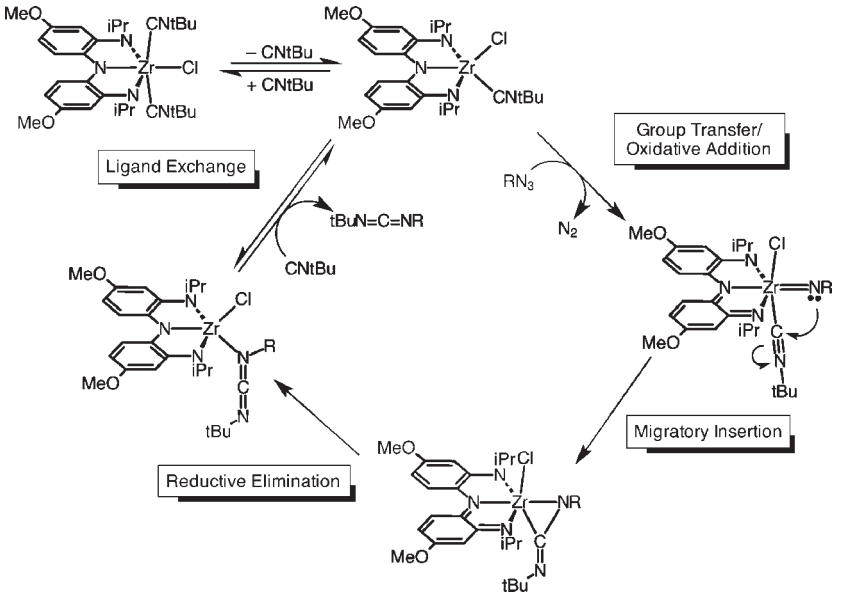

first step of the reaction is dissociation of an isocyanide to form a $[NNN^{cat}]ZrCl(CNtBu)$ species. This five-coordinate species can be oxidized by the organic azide to form the putative monomeric imide intermediate, $[NNN^{q}]ZrCl(=NR)(CNtBu)$, in the rate-determining step. It is established that early-transtion-metal imido complexes with isocyanide ligands undergo nonredox, migratory insertion reactions to form η^2-carbodiimide species.[5] In this case, the migratory insertion step disposes the complex for a second C−N bond-forming reaction, reductive elimination, which forms the C−N π bond and reduces the $[NNN^{q}]^-$ ligand back to the $[NNN^{cat}]^{3-}$ form. The final step to close the catalytic cycle is displacement of the carbodiimide product from the metal coordination sphere by an isocyanide. Because the final step is a ligand-exchange process, product buildup impedes the reaction at high conversion.

VI. NITRENE CHEMISTRY OF THE [ONO]Ta PLATFORM

The two-electron reactivity of the [ONO]Ta platform, discussed in section III, prompted further investigations into the reactivity of that system. Accordingly, oxidation of the imido dimer complex $\{[ONO^{cat}]Ta(py)(\mu\text{-NPh})\}_2$ with 2 equiv of $PhICl_2$ resulted in the formation of azobenzene and 2 equiv of $[ONO^{cat}]TaCl_2(py)$, an overall four-electron reductive elimination of azobenzene (Scheme 6).[46] Reactions carried out with substoichiometric quantities of oxidant resulted in a portion of the starting materials being carried through to the products with no evidence for the formation of a partially oxidized intermediate.

An interesting aspect of the oxidation of $\{[ONO^{cat}]Ta(py)(\mu\text{-NPh})\}_2$ by $PhICl_2$ was revealed in crossover experiments. The unoxidized dimer $\{[ONO^{cat}]Ta(py)(\mu\text{-NPh})\}_2$ is robust in solution, showing no evidence for dissociation into terminal monomeric tantalum imido complexes. In contrast, when a 1:1 mixture of $\{[ONO^{cat}]Ta(py)(\mu\text{-NPh})\}_2$:$\{[ONO^{cat}]Ta(py)(\mu\text{-N-}p\text{-tolyl})\}_2$ was oxidized with a stoichiometric quantity of $PhICl_2$, the product azobenzenes were a statistical distribution of the derivatives PhN=NPh, (*p*-tolyl)N=N(*p*-tolyl), and PhN=N(*p*-tolyl), implicating a terminal imido intermediate, plausibly $[ONO^{q}]TaCl_2(=NR)$, along the reaction pathway. In an attempt to study this putative imido intermediate, alternative routes to transfer a nitrene to $[ONO^{cat}]TaCl_2(OEt_2)$ were investigated.

One potential route to the formation of metal imido complexes is the homolytic cleavage of organic diazenes.[15,66] The addition of azobenzene to solutions of $[ONO^{cat}]TaCl_2(THF)$ or $[ONO^{cat}]TaCl_2(py)$ resulted in no reaction; however, when azobenzene was added to a benzene solution of $[ONO^{cat}]TaCl_2(OEt_2)$, the red color immediately changed to green. Solutions of the green product were paramagnetic with $\mu_{eff} = 1.37\ \mu_B$ (Evans' method[67] at 298 K); upon cooling to 188 K, the magnetic moment increased to $2.18\ \mu_B$. The addition of THF or pyridine to these green solutions resulted in an immediate and quantitative conversion to $[ONO^{cat}]TaCl_2(THF)$ or $[ONO^{cat}]TaCl_2(py)$, respectively, with the release of free azobenzene. When $[ONO^{cat}]TaCl_2(OEt_2)$ was reacted with a mixture of PhN=NPh and (*p*-tolyl)N=N(*p*-tolyl) for several hours at room temperature and then quenched with pyridine, GC/MS analysis of the organic products showed no evidence for scrambling of the diazenes, indicating that complete scission of the diazene N−N bond did not occur. Titration experiments were conducted to examine formation of the paramagnetic green product, and representative UV−vis spectroscopic data are shown in Figure 7. Upon the addition of azobenzene to solutions of $[ONO^{cat}]TaCl_2(OEt_2)$, new bands grow in at 590 and 950 nm, consistent with the semiquinonate form of the [ONO] ligand. Monitoring either band by Job's method[68] (Figure 7, inset) revealed a ratio of two tantalum complexes to one azobenzene in the green product. The data are consistent with assignment of the green species as a tantalum dimer, $\{[ONO]TaCl_2\}_2(\mu^2\text{-}N_2Ph_2)$, shown in Scheme 7. Coordination of the azobenzene between two $[ONO^{cat}]TaCl_2$ fragments should raise the azobenzene reduction potentials[69] within the range of [ONO] ligands, resulting in the transfer of one or two electrons to the azobezene and with concomitant oxidation of one or both [ONO] ligands to the semiquinonate level. The temperature dependence of μ_{eff} is consistent with the proposed

dx.doi.org/10.1021/ic200911b |*Inorg. Chem.* 2011, 50, 9849–9863

Scheme 6

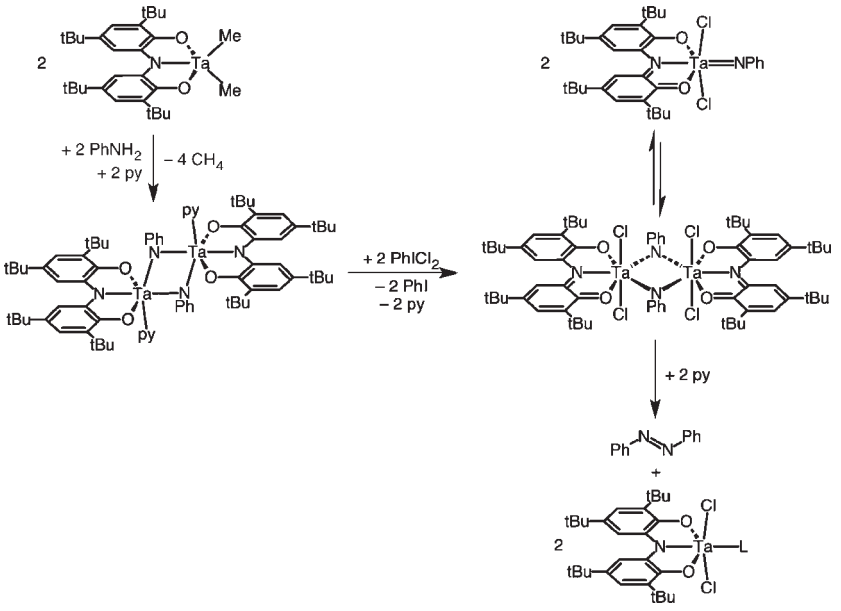

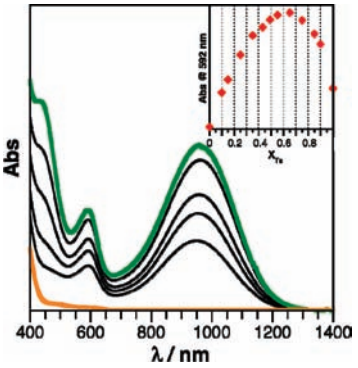

Figure 7. Changes in the electronic absorption spectrum upon titration of $[ONO^{cat}]TaCl_2(OEt_2)$ with azobenzene in benzene at 22 °C. Inset: Job's plot for the reaction of $[ONO^{cat}]TaCl_2(OEt_2)$ with azobenzene.

equilibrium formation of $\{[ONO]TaCl_2\}_2(\mu^2\text{-}N_2Ph_2)$ as a ground-state $S = 1$ species; however, we have been unable to isolate pure samples of the complex in the solid state to conduct the requisite magnetic measurements to verify this hypothesis.

Given the facile transfer of nitrene from organoazides to $[NNN^{cat}]TaCl_2$ and $[NNN^{cat}]ZrCl(L)_2$, we attempted to prepare the putative terminal imide of the [ONO]Ta platform using the same strategy. Again, aryl azides did not react with $[ONO^{cat}]TaCl_2(THF)$ or $[ONO^{cat}]TaCl_2(py)$, presumably because the organoazide cannot displace the THF and pyridine ligands from the tantalum center, even at elevated temperatures. In contrast, the addition of PhN_3 to the ether adduct, $[ONO^{cat}]TaCl_2(OEt_2)$, at 55 °C in benzene resulted in the liberation of 1 equiv of nitrogen gas (quantified by a Toepler pump) and the formation of a green solution, which returned $[ONO^{cat}]TaCl_2(py)$ in approximately 60% yield upon the addition of pyridine. Azobenzene was the organic product, formed in quantitative yield according to GC/MS analysis. The addition of excess PhN_3 to solutions of $[ONO^{cat}]TaCl_2(OEt_2)$ resulted in the release of approximately 10 equiv of N_2 and the formation of 5 equiv of azobenzene; however, upon the addition of pyridine, only a trace of $[ONO^{cat}]TaCl_2(py)$ could be isolated, with the bulk of the tantalum-containing product being $[NNN^{sq}]TaCl_3$ and an unidentified paramagnetic product. The discovery of $[ONO^{sq}]TaCl_3$ in reactions with excess organic azides suggested a decomposition pathway involving the expulsion or transfer of chlorine atoms ($Cl^{\bullet}$). To circumvent this side reaction, more strongly binding alkoxides were used to replace the chloride coligands.

Scheme 7

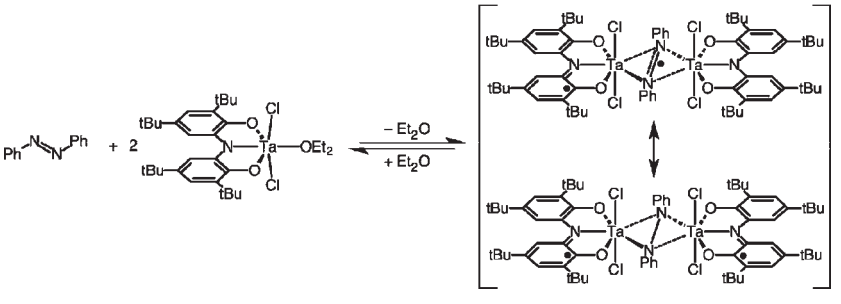

dx.doi.org/10.1021/ic200911b |*Inorg. Chem.* 2011, 50, 9849–9863

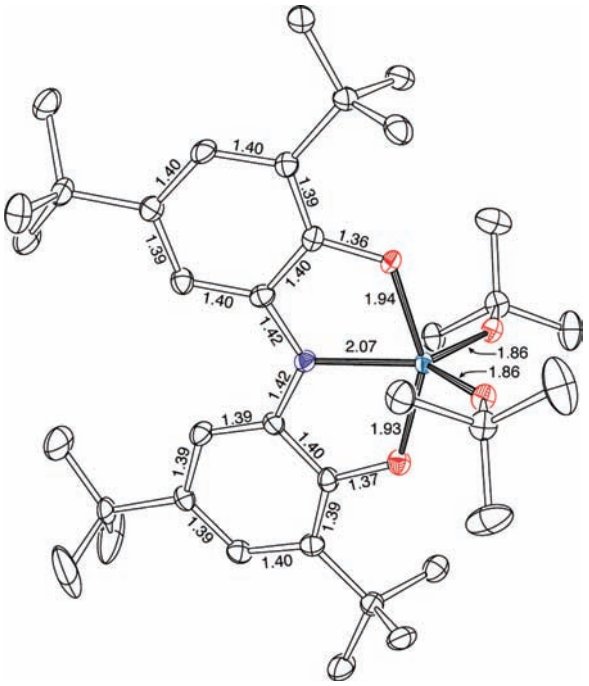

Figure 8. ORTEP diagram of $[ONO^{cat}]Ta(OtBu)_2$. Thermal ellipsoids are shown at 50% probability. Hydrogen atoms and a pentane solvent molecule are omitted for clarity. Bond distances are given in angstroms to the hundredths decimal place. Data were taken from a high-resolution structure in which the errors in C−O,N,C distances were <0.01 Å; see the Supporting Information.

Monomeric $[ONO^{cat}]Ta(OtBu)_2$ was accessible by a one-pot, two-step procedure. Attempts to prepare $[ONO^{cat}]Ta(OtBu)_2$ by the metathesis reaction of $[ONO^{cat}]TaCl_2(OEt_2)$ with LiO*t*-Bu led to an intractable product mixture. Instead, $[ONO^{cat}]$-$Ta(OtBu)_2$ was obtained by the conversion of $[ONO^{cat}]$-$TaCl_2(OEt_2)$ to $[ONO^{cat}]TaMe_2$ with MeLi followed by the dropwise addition of *t*BuOH to give the desired alkoxide as a pale-yellow solid. The ^{1}H NMR spectrum of $[ONO^{cat}]$-$Ta(OtBu)_2$ showed three singlets in the *tert*-butyl region in a 1:1:1 ratio (1.68, 1.45, and 1.18 ppm). NMR spectroscopy showed no evidence for the binding of solvent to form a six-coordinate complex. An X-ray diffraction study, undertaken on a single crystal of $[ONO^{cat}]Ta(OtBu)_2$, confirmed a five-coordinate geometry around the tantalum center. Figure 8 shows the ORTEP of $[ONO^{cat}]Ta(OtBu)_2$ along with pertinent bond distances within the metal coordination sphere and the [ONO] ligand.

The dialkoxide complex $[ONO^{cat}]Ta(OtBu)_2$ is a competent catalyst for azobenzene formation. The reaction of $[ONO^{cat}]$-$Ta(OtBu)_2$ with PhN_3 proceeded at 55 °C to form PhN═NPh (Scheme 8), albeit at a reduced rate relative to reactions employing $[ONO^{cat}]TaCl_2(OEt_2)$. Whereas reactions between $[ONO^{cat}]TaCl_2(OEt_2)$ and 1 equiv of PhN_3 were complete within 1 h at 55 °C, those between $[ONO^{cat}]Ta(OtBu)_2$ and PhN_3 took 24 h. The longer reaction times are attributed to the sterically demanding *tert*-butyl groups of the alkoxide ligands, which hinder both initial coordination of the azide to the metal center and subsequent expulsion of N_2 to form the tantalum imide.[70] Unlike the nitrene coupling reactions employing $[ONO^{cat}]TaCl_2(OEt_2)$, in the presence of excess PhN_3, $[ONO^{cat}]Ta(OtBu)_2$ does not decompose and continues to

Scheme 8

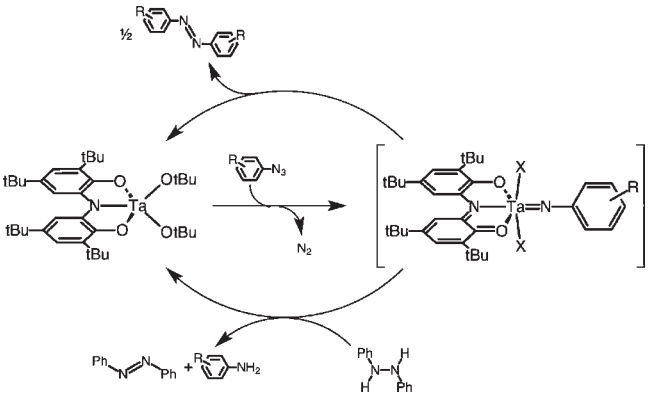

catalyze the nitrene coupling reaction, consuming 10 equiv of phenyl azide to produce 5 equiv of azobenzene over the span of 7 days at 55 °C. After complete consumption of the azide, $[ONO^{cat}]Ta(OtBu)_2$ was recovered quantitatively with no evidence for the formation of paramagnetic side products. Evidence for the intermediacy of the putative imido complex, $[ONO^{q}]$-$Ta(OtBu)_2$(═NAr), was obtained when $[ONO^{cat}]Ta(OtBu)_2$ was reacted with 1 equiv of (*p*-tolyl)N_3 in the presence of excess 1,2-diphenylhydrazine (Scheme 8). Under these conditions, no (*p*-tolyl)N═N(*p*-tolyl) or (*p*-tolyl)N═NPh was observed; instead, *p*-tolylnitrene was converted exclusively to *p*-toluidine, exactly analogous to the observed hydrazine reduction of $[NNN^{q}]TaCl_2$(═NPh).

VII. LESSONS GOING FORWARD

As with the development of any metal coordination complex for small-molecule reactivity, both electronic and steric factors have an important part to play. Within the results discussed in this work, both [ONO] and [NNN] ligands provide an appropriate redox reservoir to enable multielectron reactivity at tantalum(V) and zirconium(IV) metal centers. While experimental data indicate that these ligands prefentially hold onto the redox-active pair of valence electrons, keeping the metals in their maximum oxidation states, both chlorine and nitrene chemistry indicates that the electron pair is accessible for two-electron oxidants ($2Cl^{\bullet}$ or :NR) to add at the metal center. From this perspective, [ONO] and [NNN] ligands can be viewed as cofactors that enable redox reactions at the metal center. The differences in redox potentials observed for [NNN] and [ONO] do manifest differences in reactivity, the most obvious being in the coupling of arylnitrenes to form aryldiazenes. $[ONO^{cat}]TaX_2(OEt_2)$ (X = Cl or O*t*Bu) reacts with aryl azide to afford the aryldiazene in quantitative yield. Evidence suggests that this reaction proceeds through the initial formation of a terminal tantalum imide, $[ONO^{q}]TaX_2$(═NAr), which dimerizes to $\{[ONO^{q}]TaX_2(\mu^2\text{-NAr})\}_2$ to eliminate diazene. The elimination of diazene from the putative imido dimer is an overall four-electron reductive elimination that reduces two $[ONO^{q}]^-$ to two $[ONO^{cat}]^{3-}$. For the [NNN] ligand set, $[NNN^{cat}]ZrCl(THF)_2$ reacts with aryl azides along an analogous path to form an imide dimer with two quinonate ligands, $\{[NNN^{q}]ZrCl(\mu^2\text{-NAr})\}_2$. This imido dimer is stable indefinitely and does not extrude the aryldiazene, even at elevated

dx.doi.org/10.1021/ic200911b |*Inorg. Chem.* 2011, 50, 9849–9863

temperatures, despite having two $[NNN^q]^-$ ligands to accept the four electrons from diazene reductive elimination. It may be the case that the $[ONO^q]^-$ ligand can pull electrons away from the bridging imide ligands and force diazene elimination, whereas the $[NNN^q]^-$ ligand is not oxidizing enough to promote the reaction. Moving forward, catalyzing nitrene-transfer reactions to synthetically interesting substrates will require that the redox potentials of the ligand are balanced carefully with both the nitrene donor and the nitrene acceptor in order for the metal complex to act as a nitrene-transfer catalyst.

Ligand sterics also play an important role in controlling the coordination geometry at the metal center of these imido complexes. The differences in reactivity observed for the reaction of aryl azides with five-coordinate $[NNN^{cat}]TaCl_2$ and six-coordinate $[NNN^{cat}]TaCl_2(py)$ show that a vacant site on the metal is critical to azide activation and formation of the metal imide. The transfer of nitrene to $[NNN^{cat}]TaCl_2$ forms a six-coordinate imido complex, $[NNN^q]TaCl_2(=NAr)$, which can be reduced by 1,2-diphenylhydrazine but is unreactive with substrates that need to bind first to the metal center. Thus, to realize nitrene-transfer catalysis, there must be one open coordination site on the metal to accept nitrene from the donor and a second open coordination site on the metal imido species to bind the substrate that ultimately will accept the nitrene fragment. The chemistry of the [NNN]Zr system illustrates the pitfalls associated with these requirements. $[NNN^{cat}]ZrCl(THF)_2$ opens one coordination site to react with ArN_3 and form putative $[NNN^q]ZrCl(=NAr)(THF)$. The loss of the second THF molecule from this species generates a second open coordination site; however, dimerization of two $[NNN^q]ZrCl(=NAr)$ fragments affords an unreactive imido-bridged dimer. To effect nitrene transfer, substrate coordination must outpace dimerization of the $[NNN^q]ZrCl(=NAr)$ fragments. One way to accomplish this result is by using strong donor ligands such as isocyanides. These ligands both intercept the terminal zirconium imido species before dimerization and accept the nitrene fragment to make carbodiimides. Broadening the nitrene−acceptor substrate scope to target products such as aziridines and amines will require a strategy that slows down (or stops) the imide dimerization reaction, which, in turn, will demand redox-active ligands with more sterically demanding substituents.

VIII. EXPERIMENTAL SECTION

General Synthetic Methods. All compounds reported below are air- and moisture-sensitive, and as such all manipulations were carried out under air- and moisture-free conditions using standard Schlenk and glovebox techniques. Solvents were sparged with argon and deoxygenated and dried by passage through Q5 and activated alumina columns, respectively. To test for effective oxygen and water removal, solvents were treated with a few drops of a purple solution of a sodium benzophenone ketyl radical in THF. Aryl azides,[71,72] tertiary alkyl azides,[73,74] $[ONO^{cat}]TaCl_2(L)$,[46] and $[NNN^q]TaCl_2(=N\text{-}p\text{-tolyl})$[42] were synthesized by literature procedures.

Spectroscopic and Analytical Methods. NMR spectra were collected on Bruker Avance 600 or 500 MHz spectrometers in dry, degassed benzene-d_6 at 293 K unless otherwise noted. ^{1}H NMR spectra were referenced to tetramethylsilane using residual proteo impurities of the solvent (7.16 ppm); ^{13}C NMR spectra were referenced to tetramethylsilane using the natural abundance ^{13}C impurities of the solvent (128.06 ppm).[75] All chemical shifts are reported using the standard notation δ in parts per million. IR spectra were recorded as KBr pellets with a Perkin-Elmer Spectrum One FTIR spectrophotometer. Electronic absorption spectra were recorded as solutions in 1 cm quartz cuvettes using either a Perkin-Elmer Lambda 800 UV−vis spectrophotometer or a Perkin-Elmer Lambda 800 UV−vis spectrophotometer equipped with a near-IR detecor. EPR spectra were collected on a Bruker EMX X-band spectrometer equipped with an ER041XG microwave bridge. Spectra for EPR samples were collected using the following spectrometer settings: attenuation = 20 dB, microwave power = 2.017 mW, frequency = 9.64 GHz; sweep width = 300 G, modulation amplitude = 9.02 G, gain = 2.00×10^3, conversion time = 10.24 ms, time constant = 81.92 ms, and resolution = 2048 points. Elemental analyses were collected on a Perkin-Elmer 2400 series II CHNS/O analyzer. GC/MS data were collected using a Finnigan Trace mass spectrometer with a 30 m DB-5 column. Product concentrations were quantified using a calibration curve comprised of at least five samples of known concentration. An internal standard (biphenyl) was used to adjust for variations in the sample volume.

Electrochemical Methods. Electrochemical measurements were recorded with a Gamry G300 potentiostat using an electrochemical cell comprising a 1.5 mm diameter platinum disk electrode, a silver wire reference electrode, and a platinum wire auxiliary electrode. Cyclic voltammograms were recorded in a glovebox under an N_2 atmosphere at room temperature in CH_2Cl_2 solutions containing 1 mM analyte and 0.1 M $[Bu_4N][PF_6]$ as the supporting electrolyte. All potentials were referenced to $[Cp_2Fe]^{+/0}$ using an internal $[Cp_2Co]^{+/0}$ standard ($E^{\circ\prime}$ = −1.336 V vs $[Cp_2Fe]^{+/0}$).[76] Under our conditions, the typical solvent window is from a reductive limit of −1.20 V to an oxidative limit of +1.77 V.

Crystallographic Methods. X-ray diffraction data for $[ONO^{cat}]TaCl_2(OEt_2)\cdot 2Et_2O$, [NN(Me)N]TaMe(=N-*p*-tolyl), and $[ONO^{cat}]Ta(OtBu)_2\cdot C_5H_{12}$ were collected on single crystals mounted on glass fibers with Paratone oil using a Bruker platform diffractometer equipped with a CCD detector. Measurements were carried out at 143 K using Mo Kα radiation (λ = 0.710 73 Å), which was wavelength-selected with a single-crystal graphite monochromator. The *SMART* program package was used to determine the unit-cell parameters and for data collection. The raw frame data were processed using *SAINT* and *SADABS* to yield the reflection data file. Subsequent calculations were carried out using the *SHELXTL* program. Analytical scattering factors for neutral atoms were used throughout the analyses. Hydrogen atoms were generated in calculated positions and refined using a riding model. ORTEP diagrams were generated using *ORTEP-3* for Windows.[77] Diffraction data are shown in Table 2.

Reduction of $[NNN^q]TaCl_2(=NAr)$ with 1,2-Diphenylhydrazine. *Procedure A.* An NMR tube with a resealable Teflon valve was charged with a 0.05 M solution of $[NNN^q]TaCl_2(N\text{-}4\text{-}C_6H_4tBu)$ in C_6D_6 (200 μL, 0.01 mmol, 1 equiv), which was diluted with an additional 300 μL of C_6D_6. Next, a 0.5 M solution of 1,2-diphenylhydrazine (200 μL, 0.1 mmol, 10 equiv) was added using a microsyringe. The NMR tube was sealed, and the solution was maintained at 35 °C for 24 h. ^{1}H NMR spectroscopy was used to confirm the quantitative formation of azobenzene and *p*-*tert*-butylaniline.

Procedure B. A 1 cm quartz cuvette was charged with 2.5 mL of a 0.18 mM solution of $[NNN^q]TaCl_2(=N\text{-}p\text{-tolyl})$ in THF (0.45 μmol, 1 equiv) and 0.5 mL of a 0.14 M solution of 1,2-diphenylhydrazine in THF (70 μmol, 155 equiv). The cuvette was sealed, and spectra were recorded every 30 min at 35 °C for 12 h.

Synthesis of [NN(Me)N]TaMe(=N-*p*-tolyl). A 20 mL scintillation vial was charged with a stirbar, 100 mg of $[NNN^q]TaCl_2(=N\text{-}p\text{-tolyl})$ (0.14 mmol, 1 equiv), and 10 mL of toluene. The solution was frozen in a cold well. As the solution thawed, 183 μL of MeLi in Et_2O (1.56 M, 0.28 mmol, 2 equiv) was added dropwise. The brown solution rapidly lightened in color to orange red with concomitant precipitation

dx.doi.org/10.1021/ic200911b |*Inorg. Chem.* 2011, 50, 9849–9863

Table 2. X-ray Diffraction Data Collection and Refinement Parameters

	[ONO^{cat}]TaCl$_2$(OEt$_2$)·2Et$_2$O	[NN(Me)N]TaMe(=N-*p*-tolyl)	[ONO^{cat}]Ta(O*t*Bu)$_2$·C$_5$H$_{12}$
empirical formula	$C_{36}H_{60}Cl_2NO_4Ta$	$C_{29}H_{39}N_4O_2Ta$	$C_{41}H_{70}NO_4Ta$
fw	822.70	656.59	821.93
cryst syst	orthorhombic	monoclininc	monoclinic
space group	$P2_12_12_1$	$P2_1/n$	$P2_1/c$
a (Å)	14.5421(14)	14.9724(13)	9.9363(11)
b (Å)	16.0857(16)	9.6086(9)	20.418(2)
c (Å)	17.0730(17)	19.6981(17)	20.470(2)
α (deg)	90	90	90
β (deg)	90	102.8300(10)	92.0886(15)
γ (deg)	90	90	90
volume (Å^3)	3993.7(7)	2763.1(4)	4150.2(8)
Z	4	4	4
F(000)	1688	1320	1712
reflns collected	34 532	31 124	9852
indep reflns (R_{int})	9840 (0.0541)	6732 (0.0186)	9852 (see CIF)
GOF	1.101	1.037	1.077
R1 [$I > 2\sigma(I)$][a]	0.0582	0.0181	0.0353
wR2 (all data)[a]	0.1514	0.0473	0.0774

[a] $R1 = \Sigma||F_o| - |F_c||/\Sigma|F_o|$; $wR2 = [\Sigma[w(F_o^2 - F_c^2)^2]/\Sigma[w(F_o^2)^2]]^{1/2}$; $GOF = [\Sigma w(|F_o| - |F_c|)^2/(n - m)]^{1/2}$.

of LiCl. The solution was allowed to warm to ambient temprature over 2 h before it was filtered. Solvent removal gave a yellow solid that was triturated with 3 × 5 mL of pentane to give the product in 77% yield (0.073 g). X-ray-quality crystals were grown from saturated solutions of the complex in Et_2O chilled to −35 °C. Anal. Calcd for $C_{29}H_{39}N_4O_2Ta$: C, 53.05; H, 5.99; N, 8.53. Found: C, 52.80; H, 5.66; N, 8.40. ^{1}H NMR (600 MHz): δ 7.37 (d, 2H, $^3J_{HH}$ = 6.5 Hz, aryl-H), 6.34 (d, 2H, $^4J_{HH}$ = 2 Hz, aryl-H), 7.37 (dd, 2H, $^3J_{HH}$ = 5 Hz, aryl-H), 3.88 (sept, 2H, $^3J_{HH}$ = 5 Hz, C*H*(CH$_3$)$_2$), 3.43 (s, 6H, OCH$_3$), 3.03 (s, 3H, NCH$_3$), 1.48 (d, 12H, $^3J_{HH}$ = 5 Hz, CH(C*H*$_3$)$_2$), 1.40 (d, 12H, $^3J_{HH}$ = 5 Hz, CH(C*H*$_3$)$_2$), 0.83 (s, 3H, TaC*H*$_3$). ^{13}C{^{1}H} NMR (128 MHz): δ 160.5 (aryl-C), 150.3 (aryl-C), 130.9 (aryl-C), 128.9 (aryl-C), 126.2 (aryl-C), 126.2 (aryl-C), 122.4 (aryl-C), 100.6 (aryl-C), 102.2 (aryl-C), 54.5 (OCH$_3$), 54.0 (CH(CH$_3$)$_2$), 46.9 (TaCH$_3$), 42.7 (NCH$_3$), 25.6 (CH(*C*H$_3$)$_2$), 24.9 (CH(*C*H$_3$)$_2$).

Titration of [ONO^{cat}]TaCl$_2$(OEt$_2$) with Azobenzene. A stock solution was prepared by dissolving 37 mg of [ONO^{cat}]TaCl$_2$(OEt$_2$) (0.05 mmol) in 25 mL of benzene. A second stock solution was prepared by dissolving 66 mg of (*p*-tolyl)N=N(*p*-tolyl) (0.31 mmol) in 25 mL of benzene. Titration samples for spectroscopic analysis were prepared by combining 0.5 mL of the [ONO^{cat}]TaCl$_2$(OEt$_2$) stock solution and various quantities of the diazene stock solution and then diluting to a total volume of 5 mL with benzene ([Ta]$_{total}$ = 0.2 mM). The samples were stored at room temperature for several hours to ensure equilibration before being analyzed by UV−vis spectroscopy in 1 cm quartz cuvettes.

Synthesis of [ONO^{cat}]Ta(O*t*Bu)$_2$. A 25 mL round-bottomed flask was charged with a stirbar and a red diethyl ether (15 mL) solution containing [ONO^{cat}]TaCl$_2$(OEt$_2$) (0.141 g, 0.19 mmol, 1 equiv). The solution was frozen in a cold well, and as the solution slowly thawed, a 1.44 M solution of MeLi (262 μL, 0.38 mmol, 2 equiv) in Et_2O was slowly dripped in while the solution was stirred. After stirring for 3 h, the bright-yellow solution was lowered into a cold well and frozen. As the solution slowly thawed, *t*BuOH (0.036 mL, 0.38 mmol, 2 equiv) was slowly added dropwise while the solution was stirred. After stirring for 12 h at ambient temperature, the mixture was filtered and the volatiles were removed under reduced pressure. The resulting yellow residue was dissolved in 1 mL of pentane, filtered, and cooled (−35 °C) to afford [ONO^{cat}]Ta(O*t*Bu)$_2$ as a yellow, crystalline solid (yield 0.052 g, 41%). X-ray-quality crystals were grown from saturated solutions of pentane chilled to −35 °C for 3 days. Anal. Calcd for $C_{36}H_{58}NO_4Ta$: C, 57.67; H, 7.80; N, 1.87. Found: C, 57.36; H, 7.75; N, 1.74. ^{1}H NMR (600 MHz): δ 7.94 (s, 2H, aryl-H), 1.68 (s, 18H, *t*Bu), 1.45 (s, 18H, *t*Bu), 1.18 (s, 18H, *t*Bu). ^{13}C{^{1}H} NMR (128 MHz): δ154.5 (aryl-C), 146.1 (aryl-C), 143.5 (aryl-C), 134.4 (aryl-C), 115 (aryl-C), 110.5 (aryl-C), 84.4 (OC(CH$_3$)$_3$), 35.0 (C(CH$_3$)$_3$), 34.8 (C(CH$_3$)$_3$), 32.2 (C(*C*H$_3$)$_3$), 31.6 (C(*C*H$_3$)$_3$), 30.1 (C(CH$_3$)$_3$). UV−vis (C_6H_6) λ_{max}/nm (ε/M^{-1} cm^{-1}): 290 (15 000).

General Procedure for the Reaction of [ONO^{cat}]TaX$_2$ Complexes with Aryl Azides. In a typical experiment, an NMR tube with a resealable Teflon valve was charged with 130 μL of a 0.10 M solution of [ONO^{cat}]TaCl$_2$(OEt$_2$) in C_6D_6 (0.01 mmol, 1 equiv) and 310 μL of a 0.10 M solution of a 0.44 M solution of PhN_3 in C_6D_6 (0.1 mmol 10 equiv) and diluted with an additional 270 μL of C_6D_6 using a microsyringe. The NMR tube was sealed and heated to 55 °C in a thermostatted water bath. The reaction progress was monitored by ^{1}H NMR spectroscopy by observing consumption of PhN_3 and production of PhN=NPh. Final quantitation of the azobenzene product was confirmed by GC/MS.

Reaction of [ONO^{cat}]Ta(O*t*Bu)$_2$ with (*p*-tolyl)N$_3$ with Excess 1,2-Diphenylhydrazine. An NMR tube with a resealable Teflon valve was charged with solid [ONO^{cat}]Ta(O*t*Bu)$_2$ (0.013 g, 0.02 mmol, 1 equiv) and 590 μL of a 0.26 M solution of 1,2-phenylhydrazine in C_6D_6 (0.2 mmol, 10 equiv). After [ONO^{cat}]Ta(O*t*Bu)$_2$ dissolved, (*p*-tolyl)N$_3$ (2 μL, 0.02 mmol, 1 equiv) was added and the NMR tube was sealed and heated to 55 °C for 48 h. ^{1}H NMR spectroscopy was used to confirm the formation of 1 equiv of *p*-toluidine and 1 equiv of PhNNPh.

■ ASSOCIATED CONTENT

Supporting Information. X-ray crystallographic data in CIF format for [ONO^{cat}]TaCl$_2$(OEt$_2$)·2Et$_2$O, [NN(Me)N]TaMe (=N-*p*-tolyl), and [ONO^{cat}]Ta(O*t*Bu)$_2$·C$_5$H$_{12}$. This material is available free of charge via the Internet at http://pubs.acs.org.

dx.doi.org/10.1021/ic200911b |*Inorg. Chem.* 2011, 50, 9849–9863

AUTHOR INFORMATION

Corresponding Author
*E-mail: aheyduk@uci.edu.

ACKNOWLEDGMENT

The authors thank Dr. Joe Ziller for assistance with X-ray crystallography, Dr. John Greaves for assistance with mass spectrometry, and David Lacy for assistance with EPR spectroscopy. The NSF-CAREER program supported this work (Grant CHE-0645685). A.F.H. is a Camille Dreyfus Teacher−Scholar.

REFERENCES

(1) Wigley, D. E. *Prog. Inorg. Chem.* **1994**, *42*, 239–482.
(2) Gade, L. H.; Mountford, P. *Coord. Chem. Rev.* **2001**, *216*, 65–97.
(3) Duncan, A. P.; Bergman, R. G. *Chem. Rec.* **2002**, *2*, 431–445.
(4) Hazari, N.; Mountford, P. *Acc. Chem. Res.* **2005**, *38*, 839–849.
(5) Walsh, P. J.; Hollander, F. J.; Bergman, R. G. *Organometallics* **1993**, *12*, 3705–3723.
(6) Walsh, P. J.; Hollander, F. J.; Bergman, R. G. *J. Am. Chem. Soc.* **1988**, *110*, 8729–8731.
(7) Schaller, C. P.; Cummins, C. C.; Wolczanski, P. T. *J. Am. Chem. Soc.* **1996**, *118*, 591–611.
(8) Bennett, J. L.; Wolczanski, P. T. *J. Am. Chem. Soc.* **1997**, *119*, 10696–10719.
(9) Cundari, T. R.; Klinckman, T. R.; Wolczanski, P. T. *J. Am. Chem. Soc.* **2002**, *124*, 1481–1487.
(10) Schaller, C. P.; Wolczanski, P. T. *Inorg. Chem.* **1993**, *32*, 131–144.
(11) Blake, R. E., Jr.; Antonelli, D. M.; Henling, L. M.; Schaefer, W. P.; Hardcastle, K. I.; Bercaw, J. E. *Organometallics* **1998**, *17*, 718–725.
(12) Pugh, S. M.; Trösch, D. J. M.; Skinner, M. E. G.; Gade, L. H.; Mountford, P. *Organometallics* **2001**, *20*, 3531–3542.
(13) Gomez, M. *Eur. J. Inorg. Chem.* **2003**, *2003*, 3681–3697.
(14) Anderson, L. L.; Schmidt, J. A.; Arnold, J.; Bergman, R. G. *Organometallics* **2006**, *25*, 3394–3406.
(15) Kilgore, U. J.; Yang, X.; Tomaszewski, J.; Huffman, J. C.; Mindiola, D. J. *Inorg. Chem.* **2006**, *45*, 10712–10721.
(16) Fryzuk, M. D. *Acc. Chem. Res.* **2009**, *42*, 127–133.
(17) Thomson, R. K.; Bexrud, J. A.; Schafer, L. L. *Organometallics* **2006**, *25*, 4069–4071.
(18) Silvia, J. S.; Cummins, C. C. *J. Am. Chem. Soc.* **2009**, *131*, 446–447.
(19) Tran, B. L.; Pink, M.; Gao, X.; Park, H.; Mindiola, D. J. *J. Am. Chem. Soc.* **2010**, *132*, 1458–1459.
(20) Pierpont, C. G.; Lange, C. W. *Prog. Inorg. Chem.* **1994**, *41*, 331–442.
(21) Hendrickson, D. N.; Pierpont, C. G. *Top. Curr. Chem.* **2004**, *234*, 63–96.
(22) Lever, A. B. P.; Gorelsky, S. I. *Struct. Bonding (Berlin)* **2004**, *107*, 77–114.
(23) Poddel'sky, A. I.; Cherkasov, V. K.; Abakumov, G. A. *Coord. Chem. Rev.* **2009**, *253*, 291–324.
(24) Lever, A. B. P. *Coord. Chem. Rev.* **2010**, *254*, 1397–1405.
(25) Chaudhuri, P.; Verani, C. N.; Bill, E.; Bothe, E.; Weyhermüller, T.; Wieghardt, K. *J. Am. Chem. Soc.* **2001**, *123*, 2213–2223.
(26) Herebian, D.; Bothe, E.; Bill, E.; Weyhermüller, T.; Wieghardt, K. *J. Am. Chem. Soc.* **2001**, *123*, 10012–10023.
(27) Pierpont, C. G. *Coord. Chem. Rev.* **2001**, *216*, 99–125.
(28) Evangelio, E.; Ruiz-Molina, D. *Eur. J. Inorg. Chem.* **2005**, *15*, 2957–2971.
(29) Chirik, P. J.; Wieghardt, K. *Science* **2010**, *327*, 794–795.
(30) Ketterer, N. A.; Fan, H.; Blackmore, K. J.; Yang, X.; Ziller, J. W.; Baik, M. H.; Heyduk, A. F. *J. Am. Chem. Soc.* **2008**, *130*, 4364–4374.
(31) Blackmore, K. J.; Ziller, J. W.; Heyduk, A. F. *Inorg. Chem.* **2005**, *44*, 5559–5561.
(32) Haneline, M. R.; Heyduk, A. F. *J. Am. Chem. Soc.* **2006**, *128*, 8410–8411.
(33) Borgias, B. A.; Cooper, S. R.; Koh, Y. B.; Raymond, K. N. *Inorg. Chem.* **1984**, *23*, 1009–1016.
(34) Blackmore, K. J.; Sly, M. B.; Haneline, M. R.; Ziller, J. W.; Heyduk, A. F. *Inorg. Chem.* **2008**, *47*, 10522–10532.
(35) Blackmore, K. J.; Lal, N.; Ziller, J. W.; Heyduk, A. F. *Eur. J. Inorg. Chem.* **2009**, *6*, 735–743.
(36) Blackmore, K. J.; Lal, N.; Ziller, J. W.; Heyduk, A. F. *J. Am. Chem. Soc.* **2008**, *130*, 2728–2729.
(37) van der Vlugt, J. I.; Reek, J. N. *Angew. Chem., Int. Ed.* **2009**, *48*, 8832–8846.
(38) Gibson, V. C.; Redshaw, C.; Solan, G. A. *Chem. Rev.* **2007**, *107*, 1745–1776.
(39) Girgis, A. Y.; Balch, A. L. *Inorg. Chem.* **1975**, *14*, 2724–2727.
(40) Speier, G.; Csihony, J.; Whalen, A. M.; Pierpont, C. G. *Inorg. Chem.* **1996**, *35*, 3519–3524.
(41) Chaudhuri, P.; Hess, M.; Weyhermuller, T.; Wieghardt, K. *Angew. Chem., Int. Ed.* **1999**, *38*, 1095–1098.
(42) Nguyen, A. I.; Blackmore, K. J.; Carter, S. M.; Zarkesh, R. A.; Heyduk, A. F. *J. Am. Chem. Soc.* **2009**, *131*, 3307–3316.
(43) Schrock, R. R.; Lee, J.; Liang, L. C.; Davis, W. M. *Inorg. Chim. Acta* **1998**, *270*, 353–362.
(44) Sharma, S. K.; May, P. S.; Jones, M. B.; Lense, S.; Hardcastle, K. I.; MacBeth, C. E. *Chem. Commun.* **2011**, *47*, 1827–1829.
(45) Nguyen, A. I.; Zarkesh, R. A.; Lacy, D. C.; Thorson, M. K.; Heyduk, A. F. *Chem. Sci.* **2011**, *2*, 166–169.
(46) Zarkesh, R. A.; Ziller, J. W.; Heyduk, A. F. *Angew. Chem., Int. Ed.* **2008**, *47*, 4715–4718.
(47) Guo, Z.; Swenson, D. C.; Guram, A. S.; Jordan, R. F. *Organometallics* **1994**, *13*, 766–773.
(48) Gómez, M.; Gómez-Sal, P.; Nicolás, M. P.; Royo, P. *J. Organomet. Chem.* **1995**, *491*, 121–125.
(49) Brackemeyer, T.; Erker, G.; Fröhlich, R. *Organometallics* **1997**, *16*, 531–536.
(50) Strauch, H. C.; Wibbeling, B.; Fröhlich, R.; Erker, G.; Jacobsen, H.; Berke, H. *Organometallics* **1999**, *18*, 3802–3812.
(51) Noh, W.; Girolami, G. S. *Inorg. Chem.* **2008**, *47*, 535–542.
(52) Labauze, G.; Samuel, E.; Livage, J. *Inorg. Chem.* **1980**, *19*, 1384–1386.
(53) Masui, H.; Lever, A. B. P.; Auburn, P. R. *Inorg. Chem.* **1991**, *30*, 2402–2410.
(54) Murphy, E. F.; Murugavel, R.; Roesky, H. W. *Chem. Rev.* **1997**, *97*, 3425–3468.
(55) Uhrhammer, R.; Su, Y. X.; Swenson, D. C.; Jordan, R. F. *Inorg. Chem.* **1994**, *33*, 4398–4402.
(56) Jordan, R. F.; Dasher, W. E.; Echols, S. F. *J. Am. Chem. Soc.* **1986**, *108*, 1718–1719.
(57) Baldwin, T. C.; Huber, S. R.; Bruck, M. A.; Wigley, D. E. *Inorg. Chem.* **1993**, *32*, 5682–5686.
(58) Burckhardt, U.; Casty, G. L.; Gavenonis, J.; Tilley, T. D. *Organometallics* **2002**, *21*, 3108–3122.
(59) Schmidt, J. A. R.; Arnold, J. *Organometallics* **2002**, *21*, 3426–3433.
(60) Bhattacharya, S.; Gupta, P.; Basuli, F.; Pierpont, C. G. *Inorg. Chem.* **2002**, *41*, 5810–5816.
(61) Mayer, J. M. *Acc. Chem. Res.* **2011**, *44*, 36–46.
(62) Warren, J. J.; Tronic, T. A.; Mayer, J. M. *Chem. Rev.* **2010**, *110*, 6961–7001.
(63) Camacho-Camacho, C.; Mijangos, E.; Castillo-Ramos, M. E.; Esparza-Ruiz, A.; Vasquez-Badillo, A.; Noeth, H.; Flores-Parra, A.; Contreras, R. *J. Organomet. Chem.* **2010**, *695*, 833–840.
(64) Hanna, T. E.; Lobkovsky, E.; Chirik, P. J. *J. Am. Chem. Soc.* **2006**, *128*, 6018–6019.
(65) Dunn, S. C.; Hazari, N.; Cowley, A. R.; Green, J. C.; Mountford, P. *Organometallics* **2006**, *25*, 1755–1770.
(66) Hill, J. E.; Profilet, R. D.; Fanwick, P. E.; Rothwell, I. P. *Angew. Chem., Int. Ed.* **1990**, *29*, 664–665.
(67) Evans, D. F. *J. Chem. Soc.* **1959**, 2003–2005.

(68) MacCarthy, P. *Anal. Chem.* **1978**, *50*, 2165–2165.
(69) Klopman, G.; Doddapaneni, N. *J. Phys. Chem.* **1974**, *78*, 1825–1828.
(70) Proulx, G.; Bergman, R. G. *Organometallics* **1996**, *15*, 684–692.
(71) Smith, P. A. S.; Brown, B. B. *J. Am. Chem. Soc.* **1951**, *73*, 2438–2441.
(72) Barral, K.; Moorhouse, A. D.; Moses, J. E. *Org. Lett.* **2007**, *9*, 1809–1811.
(73) Miller, J. A. *Tetrahedron. Lett.* **1975**, *16*, 2959–2960.
(74) Sasaki, T.; Nakanishi, A.; Ohno, M. *J. Org. Chem.* **1981**, *46*, 5445–5447.
(75) Fulmer, G. R.; Miller, A. J. M.; Sherden, N. H.; Gottlieb, H. E.; Nudelman, A.; Stoltz, B. M.; Bercaw, J. E.; Goldberg, K. I. *Organometallics* **2010**, *29*, 2176–2179.
(76) Connelly, N. G.; Geiger, W. E. *Chem. Rev.* **1996**, *96*, 877–910.
(77) Farrugia, L. J. *J. Appl. Crystallogr.* **1997**, *30*, 565–565.